Transcription initiation defines kinetoplast RNA boundaries

François M. Sement[a,1], Takuma Suematsu[a,1], Liye Zhang[b], Tian Yu[a,c], Lan Huang[d], Inna Aphasizheva[a], and Ruslan Aphasizhev[a,e,2]

[a]Department of Molecular and Cell Biology, Boston University, Boston, MA 02118; [b]School of Life Science and Technology, ShanghaiTech University, Shanghai 200031, China; [c]Bioinformatics Program, Boston University, Boston, MA 02215; [d]Department of Physiology and Biophysics, School of Medicine, University of California, Irvine, CA 92697; and [e]Department of Biochemistry, Boston University, Boston, MA 02118

Edited by Brenda L. Bass, University of Utah School of Medicine, Salt Lake City, UT, and approved September 26, 2018 (received for review May 24, 2018)

Mitochondrial genomes are often transcribed into polycistronic RNAs punctuated by tRNAs whose excision defines mature RNA boundaries. Although kinetoplast DNA lacks tRNA genes, it is commonly held that in *Trypanosoma brucei* the monophosphorylated 5′ ends of functional molecules typify precursor partitioning by an unknown endonuclease. On the contrary, we demonstrate that individual mRNAs and rRNAs are independently synthesized as 3′-extended precursors. The transcription-defined 5′ terminus is converted into a monophosphorylated state by the pyrophosphohydrolase complex, termed the "PPsome." Composed of the MERS1 NUDIX enzyme, the MERS2 pentatricopeptide repeat RNA-binding subunit, and MERS3 polypeptide, the PPsome binds to specific sequences near mRNA 5′ termini. Most guide RNAs lack PPsome-recognition sites and remain triphosphorylated. The RNA-editing substrate-binding complex stimulates MERS1 pyrophosphohydrolase activity and enables an interaction between the PPsome and the polyadenylation machinery. We provide evidence that both 5′ pyrophosphate removal and 3′ adenylation are essential for mRNA stabilization. Furthermore, we uncover a mechanism by which antisense RNA-controlled 3′–5′ exonucleolytic trimming defines the mRNA 3′ end before adenylation. We conclude that mitochondrial mRNAs and rRNAs are transcribed and processed as insulated units irrespective of their genomic location.

Trypanosoma | mitochondria | transcription | RNA stability | NUDIX hydrolase

Notwithstanding their monophyletic origin, present-day mitochondria display an inexplicable diversity of transcriptional, RNA processing, and translation mechanisms. In animals and fungi, mitochondrial DNA is transcribed into polycistronic primary RNAs, which are cleaved internally (1, 2), while in plants diverse *cis* elements recruit RNA polymerases to individual genes (3). As suggested by the "tRNA punctuation" model, pre-mRNAs are liberated from polycistronic precursors via excision of flanking tRNAs by RNases P and Z (4, 5). The causative agent of African sleeping sickness, *Trypanosoma brucei*, maintains a bipartite mitochondrial genome composed of a few ∼23-kb maxicircles and thousands of ∼1-kb minicircles. Maxicircles encode 9S and 12S rRNAs, 18 tightly packed protein genes, a single *trans*-acting MURF2-II guide RNA (gRNA), and a *cis*-acting gRNA embedded into the 3′ UTR of CO2 mRNA. Minicircles produce most gRNAs required for U-insertion/deletion mRNA editing (6). Interestingly, mature rRNA and mRNA 5′ termini are monophosphorylated, while gRNAs retain triphosphate characteristic of the transcription start site (7). A putative maxicircle transcription-initiation region has been mapped to the major strand ∼1,200 nt upstream of the 12S rRNA, and the transcription is believed to proceed polycistronically (8, 9). Although the absence of mitochondrial tRNA genes (10) negates the tRNA punctuation scenario, it is commonly held that an unknown endonuclease cuts between functional sequences to liberate rRNAs and monocistronic pre-mRNAs (11, 12).

In contrast to maxicircle transcripts, gRNAs are synthesized from dedicated promoters as ∼1-kb precursors and are processed by 3′–5′ exonucleolytic trimming (13, 14). This reaction is carried out by DSS1 3′–5′ exonuclease (15) acting as a subunit of the mitochondrial 3′ processome (MPsome) (13). Recently, we established that rRNA and mRNA precursors accumulate upon knockdown of the MPsome's components (16). Hence, 3′–5′ trimming appears to be the major, if not the only, nucleolytic processing pathway. This *modus operandi*, however, would be incongruent with a polycistronic precursor containing several coding sequences: Only the 5′ region can be converted into pre-mRNA that is competent for polyadenylation and editing. Furthermore, any conceivable mechanism ought to account for the monophosphorylated 5′ termini and homogenous 3′ ends.

In this work, we demonstrate that mRNA and rRNA 5′ ends are defined by transcription initiation, while the 3′-extended primary transcripts encroach into downstream genes. We provide several lines of evidence that triphosphate is most likely converted into monophosphate by MERS1 NUDIX [for "nucleoside diphosphates linked to any moiety (x)"] hydrolase (17). Along with a MERS2 pentatricopeptide repeat (PPR) RNA-binding factor and a MERS3 subunit lacking any motifs, MERS1 constitutes a 5′ pyrophosphohydrolase complex, the PPsome. This particle targets mRNA 5′ termini in vivo and displays an in vitro hydrolase activity which is stimulated by the RNA-editing

Significance

It is held that in trypanosomes both mitochondrial DNA strands are transcribed into polycistronic precursors. An unknown endonuclease presumably cleaves primary transcripts to liberate monocistronic mRNAs. However, this model is incongruent with an established event of mRNA processing by 3′–5′ exonucleolytic degradation. Our work suggests that each gene is transcribed individually and the pre-mRNA undergoes 5′-end modification and controlled 3′-end trimming. We identified the pyrophosphohydrolase protein complex as responsible for pyrophosphate removal from the 5′ nucleoside and mRNA stabilization. We characterized antisense noncoding RNAs originating near mRNA 3′ termini and investigated their potential role in 3′-end demarcation. It is conceivable that transcription, in addition to mRNA editing and decay, plays a significant role in regulation of mitochondrial gene expression.

Author contributions: R.A. designed research; F.M.S., T.S., L.H., I.A., and R.A. performed research; F.M.S., T.S., L.Z., T.Y., I.A., and R.A. analyzed data; and F.M.S. and R.A. wrote the paper.

The authors declare no conflict of interest.

This article is a PNAS Direct Submission.

Data deposition: The RNA-sequencing and KAP-sequencing data files have been deposited in the BioProject database (https://www.ncbi.nlm.nih.gov/bioproject/) (accession no. BioProject PRJNA402081).

[1]F.M.S. and T.S. contributed equally to this work.

[2]To whom correspondence should be addressed. Email: ruslana@bu.edu.

This article contains supporting information online at www.pnas.org/lookup/suppl/doi:10.1073/pnas.1808981115/-/DCSupplemental.

Published online October 17, 2018.

substrate-binding complex (RESC) (18). The PPsome apparently functions as a "protein cap" to stabilize monophosphorylated mRNAs by interacting with the kinetoplast polyadenylation complex (KPAC) to tether 5′ and 3′ termini. Finally, we propose a mechanism by which the antisense noncoding RNAs (ncRNAs) may modulate the 3′–5′ degradation activity of the mitochondrial MPsome (13), thereby defining the 3′ ends of maxicircle-encoded mRNAs.

Results

Kinetoplast Genes Are Transcribed as Independent Units. To investigate mitochondrial RNA polymerase (MTRNAP) occupancy of the maxicircle DNA, we developed the kinetoplast affinity purification-sequencing (KAP-seq) protocol. The C-terminally tandem affinity purification (TAP)-tagged MTRNAP was expressed in an insect (procyclic) developmental form of the parasite and was verified to have been targeted to the mitochondrial matrix without appreciably impacting cell growth (*SI Appendix*, Fig. S1 *A* and *B*). The 170-kDa MTRNAP-TAP protein was incorporated into an ∼900-kDa complex (Fig. 1*A*) which was resistant to RNase and DNase treatment (*SI Appendix*, Fig. S1*C*). Live cells were cross-linked with formaldehyde (Fig. 1*B*), and DNA was fragmented by focused sonication (*SI Appendix*, Fig. S1*D*). At the ∼100-bp resolution achieved with nonstranded KAP-seq (Fig. 1*C*), MTRNAP binding was detected predominantly within the conserved gene-containing region (Fig. 1*D*). This trend is particularly instructive for adjacent genes, such as *9S* and *12S* mitochondrial rRNAs or the *ND7-CO3-cyb-A6* segment. Here, polycistronic transcription would be expected to correlate with uniform MTRNAP progression. However, the *cyb* gene clearly shows a decreased number of KAP-seq reads compared with neighboring *ND7*, *CO3*, and *A6*. In the segment devoid of annotated genes, a major occupancy peak matched the position of a previously mapped precursor of unknown function originating ∼1,200 nt upstream of the 12S rRNA (8). Although KAP-seq results do not entirely negate the polycistronic transcription model, the MTRNAP occupancy appears to correlate with the positioning of individual rRNA and protein genes and with transcripts of unknown function.

Transcription Initiation Defines the 5′ End. To corroborate independent transcription of individual genes, we performed in vivo UV cross-linking affinity purification sequencing (CLAP-seq) to identify nascent RNAs bound to transcribing RNA polymerase (Fig. 2*A*). In this application, cell extract was treated with RNases A and T1 to fragment RNA while isolated RNA protein adducts were digested on beads with 3′–5′ exonuclease RNase R. The latter step reduces overall background by degrading RNAs with 3′ ends unprotected by MTRNAP. In agreement with the DNA-binding profile, the distribution of CLAP-seq reads along the maxicircle coding region largely concurred with gene boundaries (Fig. 2*B*). Remarkably, omitting RNase A/T1 digestion enriched 5′ regions among MTRNAP-bound mRNAs (Fig. 2*C*). Statistical analysis demonstrated a significant increase in the number of reads covering the 5′ termini of 18 of 20 annotated maxicircle transcripts (Fig. 2*D* and Dataset S1, χ^2 test).

The monophosphorylated state of the mature mRNA 5′ end has been exposed by molecular cloning (19). To test directly whether positions of primary and processed 5′ ends coincide, an RNA adapter was ligated to mock- and polyphosphatase-treated RNA. This reaction converts the tri- and diphosphate termini into monophosphorylated substrate for T4 RNA ligase; therefore, an increase in read counts would reflect tri- and diphosphate occurrence. The gene-specific 5′ RACE-seq libraries were constructed from the parental cell line and from the cell line conditionally expressing a dominant-negative (DN) variant of DSS1 3′–5′ exonuclease (DSS1 DN). DSS1 repression causes the accumulation of 3′-extended gRNA, rRNA, and mRNA precursors (13, 16). Hence, we reasoned that the positions of gene-specific transcription initiation sites should not change. In the parental cell line, the polyphosphatase-dependent gains in 5′ reads indicated that 10–45% of mRNA species retain the transcription-incorporated 5′ nucleoside triphosphate (Fig. 2*E*).

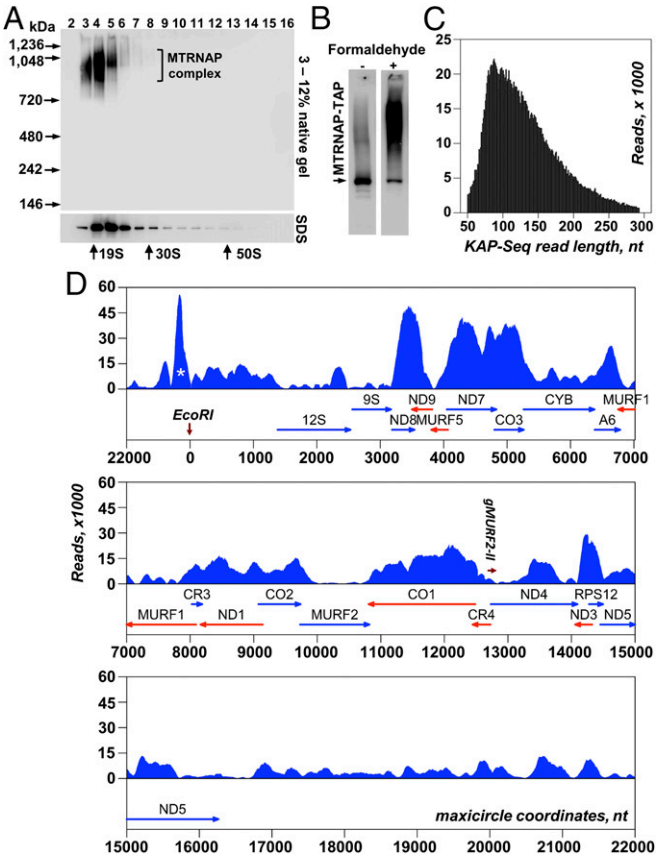

Fig. 1. RNA polymerase occupancy conforms to individual gene boundaries. (*A*) Glycerol gradient fractionation of the MTRNAP complex. Mitochondrial lysate from cells expressing TAP-tagged MTRNAP was separated in a 10–30% glycerol gradient. Each fraction was resolved on native and denaturing gels. The TAP fusion protein was detected by immunoblotting. (*B*) Formaldehyde-induced cross-linking of MTRNAP. Live cells expressing MTRNAP-TAP were cross-linked with formaldehyde, extracted, and separated on SDS gel. (*C*) Length distribution of KAP-seq reads that mapped to the maxicircle. (*D*) MTRNAP occupancy of the maxicircle. Genes located on major and minor strands are diagrammed by blue and red arrows, respectively. Read counts and maxicircle coordinates (GenBank accession no. M94286.1) are shown starting at the unique EcoRI site. The peak in the noncoding region upstream of 12S rRNA corresponding to the major precursor of unknown function (8) is marked by an asterisk.

Considering all mRNAs as a group, the combined gain in supporting reads is statistically significant with a P value of 0.006372 in a paired t test. By examining 5′ ends at a single-nucleotide resolution, we found that the sequences remained unaltered in DSS1 DN cells, while some transcripts became enriched in polyphosphatase-treated RNA. Importantly, correlation analysis confirmed that the 5′ termini derived from mono- or di-/triphosphorylated RNAs were virtually identical in parental and DSS1 DN cell lines (Dataset S1). These data corroborate synthesis of 5′-defined RNAs and an absence of 5′–3′ exonucleolytic processing (Fig. 2*F*). Collectively, in vivo analysis of MTRNAP occupancy, sequencing of nascent transcripts, and determination of 5′-end positions and phosphorylation states demonstrate that individual genes are transcribed as independent units.

Identification of the 5′ PPsome. In mitochondria of trypanosomes, a monophosphorylated 5′ end is apparently produced by pyrophosphate removal, but the cognate activity and functional implications of triphosphate into monophosphate conversion are uncertain. To address these questions, we focused on NUDIX hydrolases, enzymes that cleave nucleoside diphosphates linked to any moiety, including RNA. A survey of the *T. brucei* genome

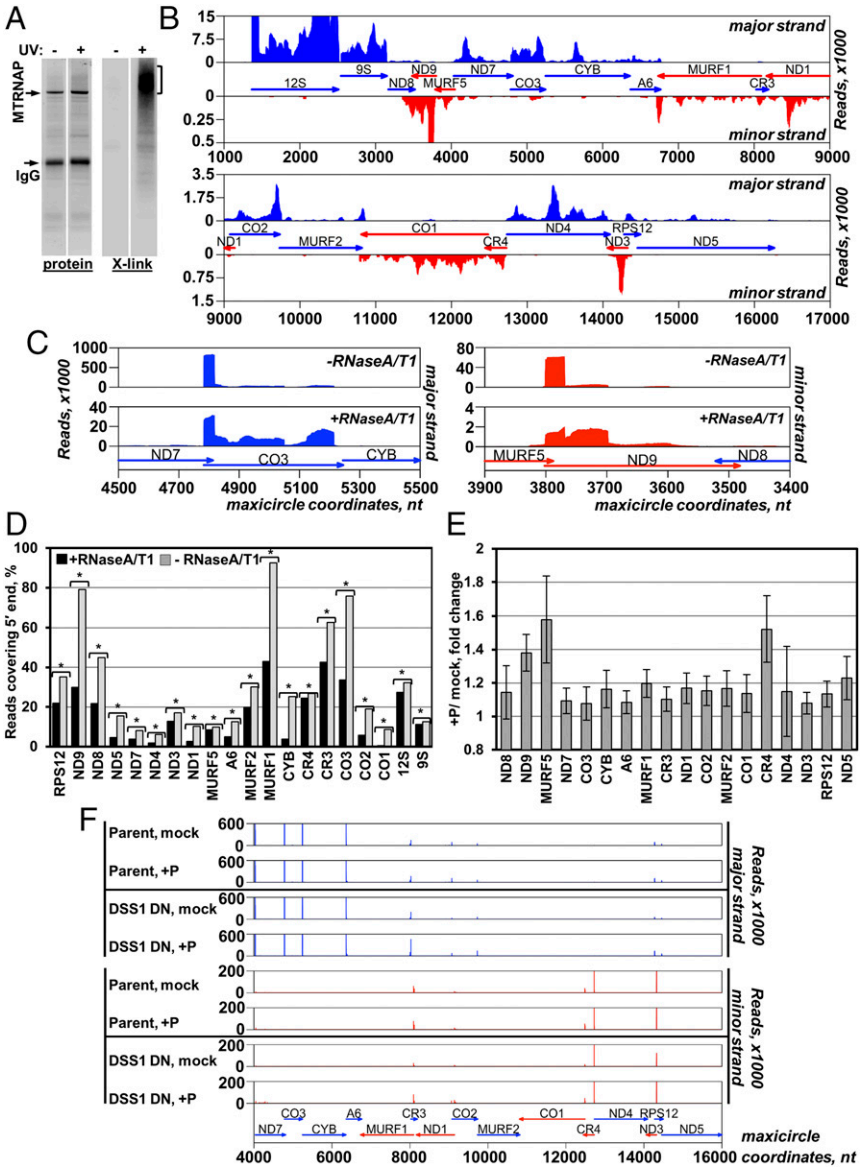

Fig. 2. Mature 5′ termini correspond to transcription initiation sites. (*A*) CLAP. The MTRNAP-TAP purification from mock-treated (–) or UV-irradiated (+) parasites was accompanied by RNase A and T1 fragmentation in the extract, treatment with RNase R on beads, and radiolabeling of the cross-linked RNA. Adducts were separated by SDS/PAGE, transferred onto nitrocellulose membrane, and visualized by Sypro Ruby staining (Thermo Fisher Scientific) (protein) or by exposure to a phosphor storage screen (X-link). RNA was eluted from the areas indicated by the bracket and was sequenced. (*B*) Positioning of nascent RNAs. MTRNAP CLAP reads were mapped to the coding region of the maxicircle. Predicted genes on major (blue) and minor (red) strands, read counts, and maxicircle coordinates are indicated. (*C*) Representative examples of reads redistribution upon omitting RNase A/T1 treatment during MTRNAP CLAP. (*D*) Enrichment of mRNA and rRNA 5′ regions in MTRNAP-bound RNAs. The percentage of CLAP reads covering the 5′ terminus was calculated for each gene. Asterisks denote a significant 5′-end increase (χ^2 test, $P < 0.01$). (*E*) Detection of individual triphosphorylated transcripts. Polyphosphatase (+P)-dependent 5′-end enrichment was calculated for parental cells from normalized read counts in polyphosphatase-treated and mock-treated samples. SDs between four biological replicates are shown. (*F*) Mapping the 5′ ends of maxicircle transcripts. The 5′ end of each RACE-seq read was plotted on major (blue) and minor (red) maxicircle strands. Pearson's correlation coefficients between global 5′ RACE profiles in parental and DSS1 DN backgrounds from four biological replicates are provided in Dataset S1; $P < 0.001$.

identified five potential NUDIX-like proteins (20), of which MERS1 is targeted to the mitochondrion (21). MERS1 was initially identified by copurification with MRP1/2 RNA chaperones, but its function remained unclear (17). To place this enzyme into a functional context, we assessed MERS1 interactions by separating mitochondrial complexes on a glycerol gradient and native gel. The 44.4-kDa polypeptide was chiefly incorporated into an ∼1-MDa (30S) complex that extended into heavier fractions (35S–50S); a minor ∼190-kDa MERS1-containing particle was also detected (Fig. 3*A*, *Left*). Notably, pretreatment of lysate with RNase I released MERS1 from the high molecular mass complex as a discrete ∼160-kDa particle (Fig. 3*A*, *Middle*). We also noticed that the high molecular mass MERS1 complex closely resembles patterns displayed by GRBC1/2 proteins (Fig. 3*A*, *Right*). These proteins are responsible for gRNA stabilization (17) and belong to the gRNA-binding module (GRBC) within the RESC. Two other RESC modules, the RNA-editing mediator complex (REMC) and the polyadenylation mediator complex (PAMC), engage the U-insertion/deletion mRNA-editing core complex (RECC) and KPAC, respectively (18).

To gain a higher-resolution view, we performed LC-MS/MS analysis of tandem affinity-purified MERS1 and of two proteins that were most abundant in the MERS1 fraction. These were the PPR-containing protein MERS2 (Tb11.02.5120) and MERS3 polypeptide lacking any discernible motifs (Tb927.10.7910) (Fig. 3 *B* and *C*). The established components of the RESC (GRBC1 and GRBC5), RNA-editing core (RET2 TUTase), and KPAC (KPAP1 poly(A) polymerase) complexes were also purified along with small (S17) and large (L3) ribosomal subunits (Dataset S2). An interaction network built on normalized spectral abundance factors (NSAF) (22) predicted that MERS1 interacts with MERS2 and, through MERS3, connects mostly to the REMC module within the RESC (Fig. 3*D*). To validate MERS3 as an adaptor between the PPsome and RESC complexes and to test its proximity to the REMC module, we expressed a MERS3–BirA* biotin ligase fusion protein and identified in vivo biotinylated polypeptides by mass spectrometry (BioID) (23). In agreement with interaction network predictions, the REMC proteins RGG2 and REMC5A were the most abundant among the biotinylated RESC subunits, followed by GRBC and PAMC components (Fig. 3*E*). Notably, BioID experiments detected relatively high quantities of the MRP1/2 complex, which rationalizes the original discovery of MERS1 by copurification with this enigmatic RNA chaperone (21).

To validate direct MERS1–MERS2 and MERS1–MERS3 interactions, we performed coimmunoprecipitations from reticulocyte lysates programmed for the synthesis of binary or ternary combinations

BIOCHEMISTRY

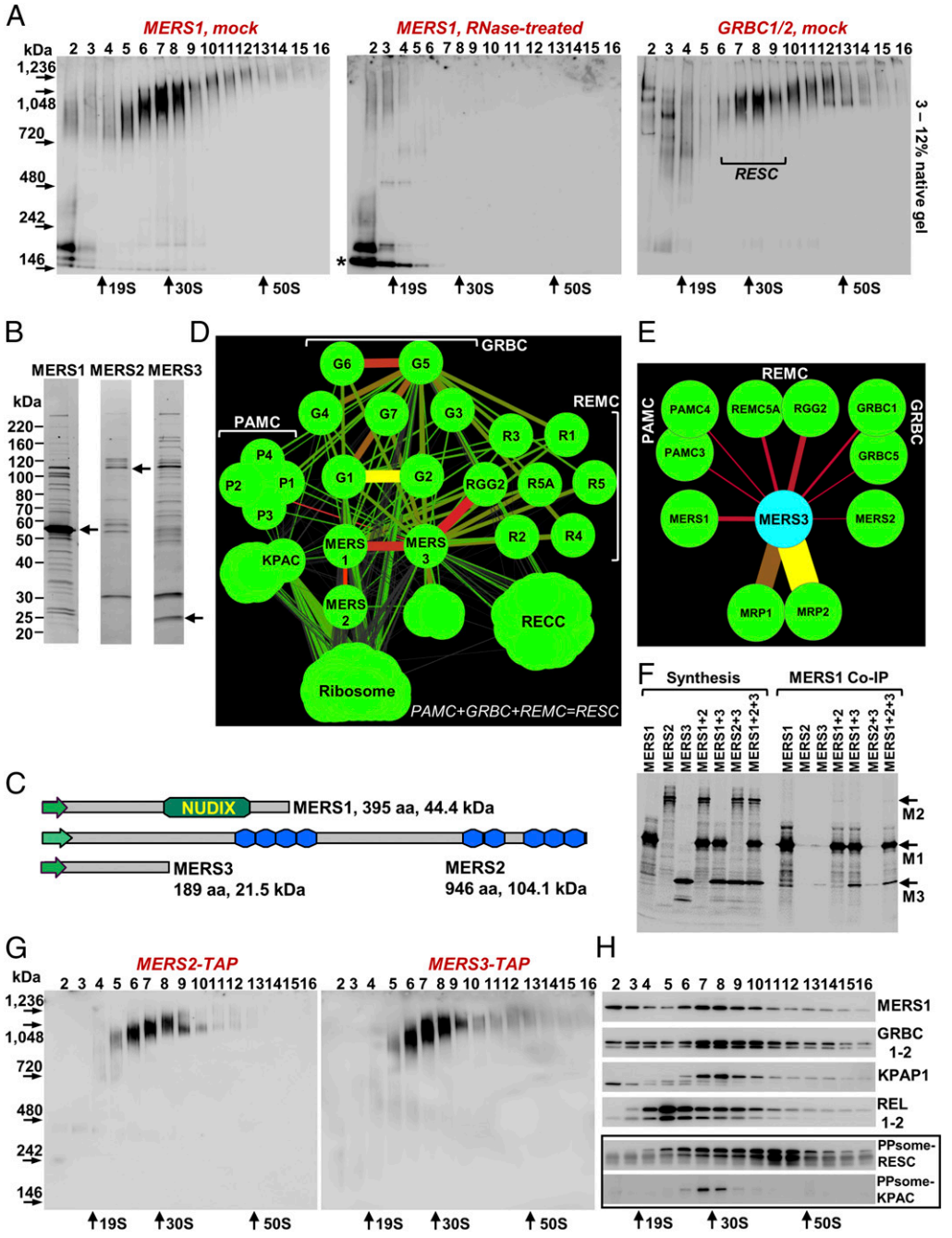

Fig. 3. The PPsome interacts with mRNA-processing complexes. (*A*) MERS1 interacts with a high molecular mass complex via RNA. Mock- and RNase-treated mitochondrial lysates were fractionated on 10–30% glycerol gradients, and each fraction was further resolved on native 3–12% Bis-Tris polyacrylamide gel. (*Left* and *Middle*). The MERS1 complex was detected by immunoblotting with polyclonal antibodies. The MERS1 particle released by RNase treatment is marked by asterisk. (*Right*) The RESC was visualized with anti-GRBC1/2 antibodies. (*B*) TAP of PPsome components. Purified MERS1, -2, and -3 fractions were separated on SDS/PAGE and stained with Sypro Ruby. Bait proteins are indicated by arrows. (*C*) Domain organization of major PPsome subunits. The MERS1 hydrolase domain and PPRs in MERS2 are diagrammed. Green arrows show mitochondrial-targeting peptides. (*D*) Interactions network of MERS1, -2, and -3 and KPAC, RESC, RECC, and the ribosome. The RESC is composed of GRBC, REMC, and PAMC modules (18). Their subunits are marked as G, R, and P, respectively. The edge thickness correlates with the NSAF value. Gene IDs and names are provided in Dataset S2. (*E*) The MERS3 proximity network determined by BioID. Edges between PPsome and RESC subunits reflect their NASF. The entire list of proteins identified by in vivo biotinylation–mass spectrometry is presented in Dataset S3. (*F*) In vitro reconstitution of the PPsome. Synthesis: Individual proteins or their combinations were synthesized in a coupled transcription–translation reticulocyte system supplemented with [^{35}S]methionine. MERS1 Co-IP: Immunoprecipitations were performed with immobilized anti-MERS1 polyclonal antibody. Coprecipitated proteins were separated by 8–16% SDS/PAGE and were exposed to a phosphor storage screen. The positions of PPsome subunits are indicated by arrows as M1, M2, and M3. (*G*) Complex association of MERS2 and MERS3 subunits. Extracts from cells expressing respective C-terminally TAP-tagged proteins were fractionated as in *A*. Fusion proteins were detected by immunoblotting with antibody against the calmodulin-binding peptide tag. (*H*) Interactions between the PPsome, RESC, and KPAC complexes. Gradient fractions were separated on denaturing PAGE and were probed for MERS1, GRBC1/2, and KPAP1 poly(A) polymerase. The RECC was detected by self-adenylation of REL1 and REL2 ligases in the presence of [α-^{32}P]ATP. Immunoblotting with anti-GRBC1/2 and anti-KPAP1 antibodies was used to detect the RESC and KPAC, respectively, in samples immunoprecipitated with anti-MERS1 antibody (framed panels).

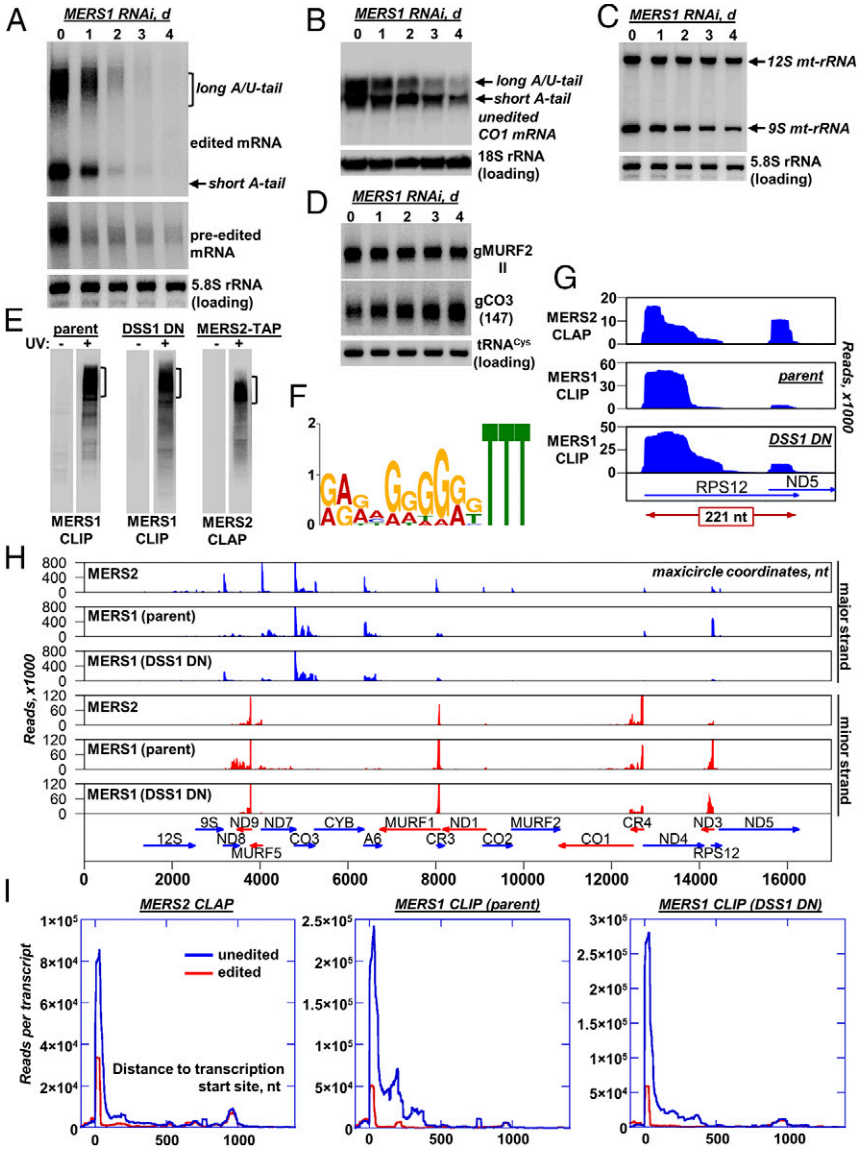

Fig. 4. MERS1 is essential for mRNA and 9S rRNA stability. (*A*) Impact of MERS1 RNAi knockdown on pan-edited mRNA. Edited and pre-edited forms of representative RPS12 mRNA were analyzed by Northern blotting. RNAi was induced with tetracycline, and samples were collected daily. MERS1 down-regulation was verified by immunoblotting (Fig. 5*D*). (*B*) MERS1 knockdown effects on unedited mRNAs were assessed by Northern blotting. (*C*) rRNA Northern blotting in MERS1 RNAi cells. (*D*) gRNA Northern blotting in MERS1 RNAi cells. (*E*) Isolation of UV-induced MERS1- and MERS2-RNA cross-links. CLIP: MERS1 was immunoaffinity-purified from parental and DSS1 DN cells using immobilized polyclonal antibody. CLAP: TAP-tagged MERS2 was purified by affinity pulldown. RNA was fragmented by RNases A and T1, radiolabeled, released from the cross-link (indicated by brackets), and sequenced. (*F*) MERS2 in vivo binding motif. The MEME algorithm was applied to predict the consensus MERS2-binding site. Transcript-specific occurrences are provided in Dataset S4. (*G*) MERS2 CLAP and MERS1 CLIP reads were aligned to a representative maxicircle region. (*H*) PPsome-binding sites in the maxicircle. MERS1 CLIP and MERS2 CLAP reads from parental and DSS1 DN cell lines were mapped to the gene-containing region. Annotated mitochondrial transcripts, read count scales, and maxicircle coordinates are indicated. (*I*) Composite distribution of PPsome complex-binding sites in mitochondrial mRNAs. The reads were aligned to unedited (blue) and fully edited (red) sequences. Read counts located 1,000 nt downstream and 100 nt upstream of the 5′ end in each transcript were collected in 1-nt bins. The average coverage across all maxicircle genes was plotted.

(Fig. 3*F*). When methionine residues were accounted for, MERS1 and MERS3 formed a stoichiometric complex; MERS1–MERS2 binding was apparently less stable but was still detectable after stringent washes. It seems possible that PPsome assembly may require the participation of an RNA component or additional protein factor(s). Furthermore, Fig. 3*G* shows that TAP-tagged MERS2 and MERS3 are confined to a high molecular mass complex matching the size of MERS1-contaning particles. Based on these results, we designated a complex of MERS1, -2, and -3 proteins as the mitochondrial 5′ PPsome. Finally, coimmunoprecipitations in glycerol gradient fractions confirmed interactions between the PPsome, RESC, and KPAC (Fig. 3*H*). Collectively, fractionation and reconstitution studies indicate that the PPsome engages in RNA-mediated interactions with the RESC and KPAC.

PPsome Binding Stabilizes Messenger RNAs. In *T. brucei*, unedited and edited mRNAs exist in two forms distinguished by 3′ modification patterns: a short A-tail (20–25 nt) and a bimodal 200- to 300-nt-long A/U-tail in which the short A-tail is extended into A/U heteropolymer (24–26). Pre-edited mRNAs possess only short A-tails, while rRNAs and gRNAs are uridylated. Polyadenylation plays a key role in mRNA stabilization (16, 25, 27), while the contribution of the 5′ processing remains unexplored. MERS1 RNAi knockdown triggered rapid decline of pre-edited and edited RPS12 (Fig. 4*A*) and unedited CO1 mRNA (Fig. 4*B*). 9S rRNA was also moderately down-regulated, while 12S rRNA remained unchanged (Fig. 4*C*). gRNA for the moderately edited MURF2 mRNA remained steady, while gRNA participating in pan-editing of CO3 mRNA increased in abundance by approximately twofold (Fig. 4*D*). To test whether accelerated mRNA and 9S rRNA decay in MERS1 RNAi cells may account for the observed changes in steady-state levels, we performed a real-time decay assay in which MERS1 was depleted by RNAi, and transcription was then blocked with ethidium bromide and Actinomycin D (14). Decay kinetics demonstrated that MERS1 knockdown causes moderate stabilization of short- and long-tailed edited mRNA forms but accelerated degradation of pre-edited mRNA (*SI Appendix*, Fig. S2). Hence, the decline of the pre-edited precursor causes the loss of edited mRNA. The rRNA decay kinetics were less instructive; it appears that the down-regulation of 9S rRNA may have been caused by the loss of mitochondrially encoded RPS12 protein (28), an integral structural component of the decoding center (29). Conversely, representative gRNAs for pan-edited RPS12 and CO3 mRNAs were stabilized. This effect agrees with gRNA up-regulation in genetic backgrounds with compromised RNA editing (18). Thus, MERS1 is essential for mRNA stability but is dispensable for rRNA and gRNAs maintenance.

mRNA stabilization by KPAC has been linked to kinetoplast polyadenylation factor 3 (KPAF3) binding near the 3′ end and A-tailing by KPAP1 (16, 25). To distinguish whether the PPsome binds near 5′ triphosphate or, similarly to KPAC, to the 3′ end, we identified the PPsome-binding sites by in vivo UV cross-linking (Fig. 4*E*). The similar sequences derived from MERS1 cross-linking immunoprecipitation (CLIP) and MERS2 CLAP (Pearson correlation score 0.774, $P = 2.2 \times 10^{-16}$) indicate their binding to the purine-rich sites, with a bias for three uridines at the 3′ end (Fig. 4*F* and Dataset S4). Importantly, the PPsome binds chiefly to the 5′ extremity of annotated mRNAs (Fig. 4 *G* and *H*), while less than 1% of MERS1 or MERS2 cross-links could be mapped exclusively to minicircle-encoded gRNAs (Dataset S4). Finally, CLIP experiments performed in DSS1 DN cells showed that PPsome-binding patterns remain unaltered (Fig. 4 *H* and *I*) notwithstanding the accumulation of 3′-extended precursors upon DSS1 repression (16). Together, these results indicate that the PPsome is involved in recognizing specific sequences adjacent to the transcription-generated 5′ end and in preventing mRNA degradation.

RESC Stimulates PPsome Activity. NUDIX-like activity would be expected to remove pyrophosphate or to sequentially hydrolyze γ- and β-phosphates from the 5′ end of a primary transcript (30). However, recombinant MERS1 purified from bacteria was inactive. Partial multiple-sequence alignment of the "NUDIX box" from trypanosomal, bacterial, and human enzymes identified replacement of a conserved catalytic glutamic acid residue by a threonine in MERS1 (Fig. 5*A*). This substitution is invariant in *Trypanosoma* and *Leishmania* species. To establish whether complex association is required to activate MERS1 and to determine the nature of the leaving group, we performed an enzymatic assay with MERS1 purified from mock- and RNase-treated mitochondrial lysates. The time-dependent accumulation of pyrophosphate demonstrated that the MERS1 complex indeed possesses the expected pyrophosphohydrolase activity (Fig. 5*B*), although at present we cannot definitively assign this activity to MERS1 polypeptide. However, RNA digestion in the extract virtually eliminated this activity despite similar levels of MERS1 polypeptide in purified samples (Fig. 5*C*). We hypothesized that RNA-mediated interaction between the PPsome and the RESC is required to activate MERS1 hydrolase (Figs. 3*A* and 5*C*). To explore this hypothesis, RESC variants purified via GRBC5 and RGG2 subunits and the large ribosomal subunit as control were tested in an enzymatic assay. Remarkably, RESC isoforms displayed pyrophosphohydrolase activity (Fig. 5*D*) correlative with MERS1 abundance in GRBC5 and RGG2 preparations (Fig. 5*E*).

MERS1 down-regulation by RNAi led to mRNA and 9S rRNA decline (Fig. 4 and *SI Appendix*, Fig. S3) and cell growth arrest (Fig. 5*F*), indicating that the PPsome is essential for mRNA and 9S rRNA stabilization (*SI Appendix*, Fig. S2). Knockdowns of MERS2 and MERS3 expression showed that the encoded proteins are also required for normal growth and that their loss affects several edited mRNAs (*SI Appendix*, Fig. S3). However, protein depletion may cause a phenotype due to the loss of intrinsic activity or by preventing the assembly of a functional complex. To verify MERS1 enzymatic identity and to address the functional significance of the triphosphate-to-monophosphate conversion, we generated procyclic cell lines for conditional *MERS1* knockin. In these backgrounds, one allele is disrupted; then a *tet* repressor-controlled TAP-tagged copy of a functional gene is introduced into the rRNA locus and is kept actively expressed by maintaining drug in the medium. Then the second allele is replaced with a cassette expressing either a functional or an inactive (E257A, E258A) gene (*SI Appendix*, Fig. S4*A*). Upon tetracycline withdrawal, the *tet* repressor blocks the ectopic expression. As MERS1-TAP gradually declines, the parasite's survival relies on the functionality of the mutated MERS1. In these settings, monoallelic MERS1 expression was sufficient to sustain cell division, while the active-site mutations led to a pronounced growth-inhibition phenotype (Fig. 5*F*). This provides additional genetic evidence that MERS1 is the most likely source of hydrolase activity in the PPsome complex.

Northern blotting of pan-edited (RPS12), moderately edited (*cyb*), and unedited (CO1) mRNAs along with rRNAs (Fig. 5 *G* and *H*) and qRT-PCR (*SI Appendix*, Fig. S4*B*) confirmed the virtually identical impacts of mutated MERS1 monoallelic expression and depletion of an endogenous protein by RNAi (Fig. 4). In addition, instructive differences were observed between pan- and moderately edited RNAs. In pan-edited RPS12 mRNA, editing events occur within ∼20 nt of the polyadenylation site and expand toward the 5′ end, nearly doubling mRNA length in the process (31, 32). In moderately edited *cyb* mRNA, 34 uridines are inserted adjacent to the PPsome-binding site at the 5′ end. In contrast to RPS12 mRNA, pre-edited *cyb* transcript accumulated, while the edited form declined. Thus, PPsome binding may reciprocally stimulate editing in the proximity of the 5′ end by recruiting the RESC.

5′ Pyrophosphate Hydrolysis and 3′ Adenylation Are Independent Events. The mechanism of 5′-end formation described above resolves the long-standing observation of monophosphorylated mRNAs and rRNAs and negates the hypothetical endonuclease involvement. The scarcity of PPsome-recognition sites in gRNAs also explains the triphosphorylated status of these molecules. Pyrophosphate removal and PPsome deposition at the 5′ end apparently block mature mRNA degradation by DSS1 3′–5′ exonuclease but not 3′–5′ precursor processing by the same activity. It follows that polyadenylation factors binding at the properly trimmed 3′ end and polyadenylation by KPAP1 are required (16, 25) but are not sufficient for mRNA stabilization. Based on a RESC-mediated link between the PPsome and KPAC (Fig. 3), we hypothesized that MERS1-dependent mRNA stabilization is contingent upon accurate 3′-end formation and polyadenylation. To investigate whether MERS1 repression compromises mRNA stability by interfering with 3′ adenylation, 3′ RACE RNA-seq libraries were constructed to map unmodified, adenylated, and uridylated termini in parental, MERS1 RNAi, and DSS1 DN cell lines. As expected, DSS1 repression led to a decline in adenylated 3′ ends and an increase in unmodified precursors. Conversely, MERS1 RNAi exerted only minor global effects on mRNA polyadenylation (Fig. 6*A*). Positioning (Fig. 6*B*) and nucleotide composition (Fig. 6*C*) of functional A-tails and cryptic 3′ modifications (truncated RNAs with unmodified tails, mixed tails and U-tails) also remained unaltered in pan-edited RPS12 mRNA. A summary of mature 5′ and 3′ termini determined by RACE-seq experiments is presented in Dataset S5. We conclude that MERS1 knockdown does not affect 3′ adenylation. Additionally, detection of uniform monophosphorylated termini in KPAP1 poly(A) polymerase (25) and DSS1 (16) knockdowns established that blocked 3′ adenylation or trimming do not impact PPsome activity. Although the 5′ and 3′ processing events occur independently, the RESC-mediated interaction between the PPsome and the KPAC occupying the respective termini apparently protects RNA against degradation by DSS1 exonuclease.

Antisense Transcription Defines the Mature 3′ End of Maxicircle-Encoded RNAs. Accurate precursor trimming by DSS1 is required for KPAF3 binding to the 3′ end and recruitment of KPAP1 poly(A) polymerase (16). The ensuing A-tailing and bridging between the KPAC and the PPsome likely lead to mRNA stabilization. However, KPAF3 binding is incapable of stopping 3′–5′ degradation at a precise position (16). To determine the mechanism of mRNA 3′-end formation, we hypothesized that antisense transcription near the mRNA 3′ end yields ncRNAs capable of impeding DSS1 activity. In this scenario, the 5′ end of an antisense RNA would define the position of the mRNA 3′ end. The 5′ RACE RNA-seq library was constructed from mock- and polyphosphatase-treated RNA to identify potential antisense transcription initiation sites near annotated mRNA 3′ termini in parental, MERS1 RNAi, and DSS1 DN backgrounds. By juxtaposing 3′ RACE-derived mRNA polyadenylation sites and 5′ RACE-generated antisense transcription initiation composite profiles, we detected consistent initiation signals extending inward from canonical 3′ termini (Fig. 7*A*, *SI Appendix*, Fig. S5, and

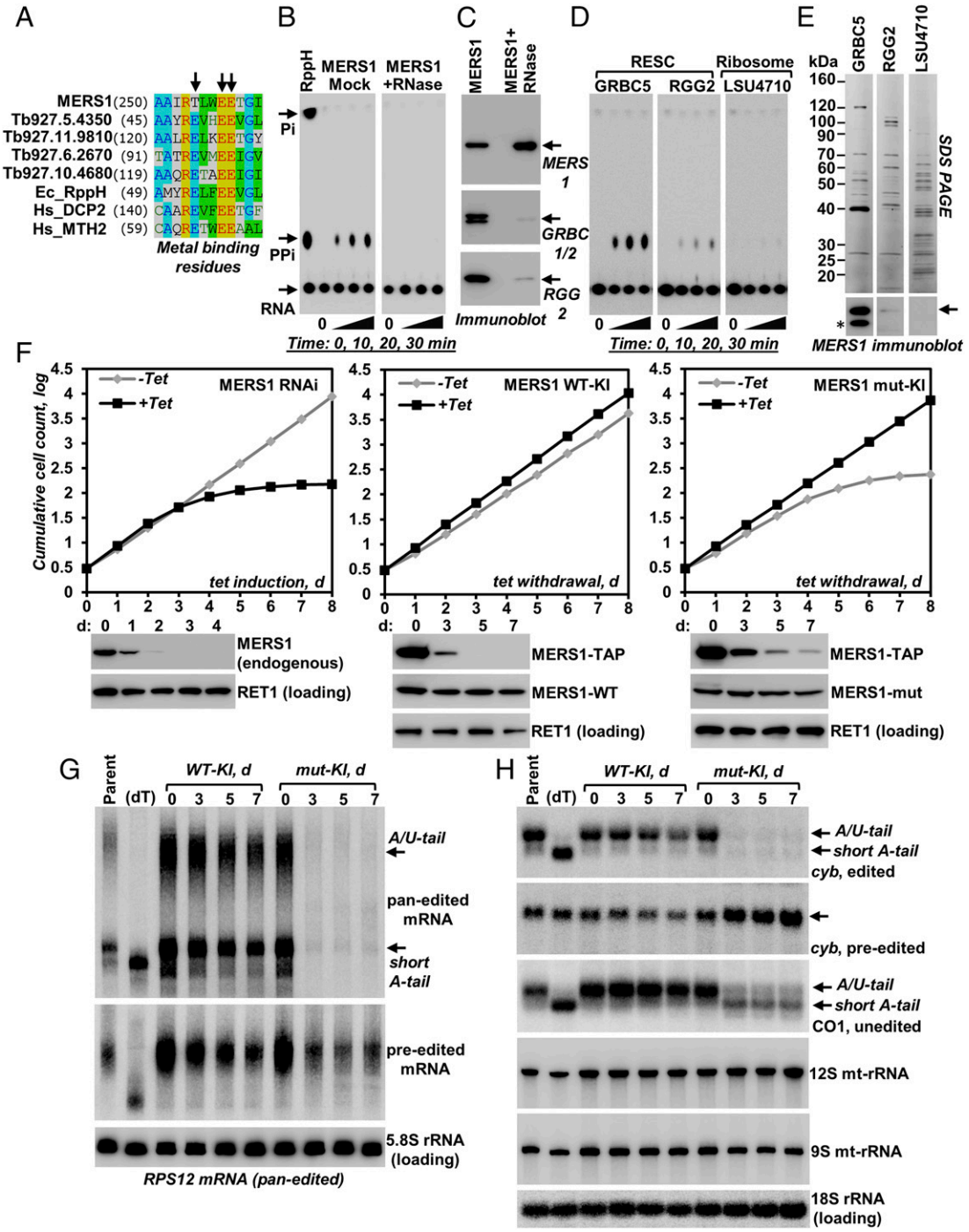

Fig. 5. The RESC stimulates MERS1 activity. (*A*) Partial alignment of NUDIX motifs from trypanosomal, bacterial, and human pyrophosphohydrolases. EC_RPPH, *Escherichia coli* RppH (WP_088540307.1); HS_DCP2, *Homo sapiens* Dcp2 (NP_001229306.1); HS_MTH2, *H. sapiens* Mth2 (NP_060753.1). The position of the first amino acid in the alignment is provided in parentheses. Metal-binding glutamic acid residues are shown by arrows. (*B*) Pyrophosphohydrolase activity of the purified PPsome. MERS1 was tandem affinity purified from mock- and RNase-treated mitochondrial extracts. Equal volumes of purified samples were incubated with the [γ-^{32}P]-labeled triphosphorylated ND8 mRNA 5′ fragment. Reaction products were separated by TLC along with those produced by RppH NUDIX hydrolase from *E. coli*. (*C*) Immunoblotting of MERS1 fractions used in the pyrophosphohydrolase activity assay in *B*. (*D*) Pyrophosphohydrolase activity in RESC isoforms and the ribosome. Complexes were affinity-purified via the indicated subunits and were incubated with the [γ-^{32}P]-labeled ND8 mRNA fragment. (*E*) MERS1 relative abundance in RESC isoforms and in the ribosome. Denaturing PAGE profiles of purified complexes and MERS1 immunoblotting are shown. Cross-reactivity of polyclonal antibodies raised against 6-His–tagged recombinant MERS1 with likewise tagged GRBC5 bait is shown by an asterisk. (*F*) Cell-growth kinetics of MERS1 RNAi and conditional knockin (KI) cell lines. RNAi was induced with tetracycline to down-regulate endogenous MERS1. In the knockin, the drug was withdrawn (zero time point) to suppress conditional MERS1-TAP expression in knockin cells. One endogenous allele constitutively expressed functional (WT-KI) or inactive (mut-KI, E257A, E258A) MERS1 proteins, while the other allele was disrupted (*SI Appendix*, Fig. S4*A*). RNAi repression and conditional (MERS1-TAP) and constitutive (MERS1-WT and MERS1-mut) expression were verified by Western blotting. (*G*) Effects of the loss of MERS1 enzymatic activity on pan-edited mRNA. Pre-edited and edited forms of RPS12 mRNA were detected by Northern blotting. (dT), RNA was treated with RNase H in the presence of oligo(dT) 20-mer to remove short A-tails and long A/U-tails. (*H*) Effects of the loss of MERS1 enzymatic activity on moderately edited *cyb* mRNA, unedited CO1 mRNA, and 9S and 12S rRNAs.

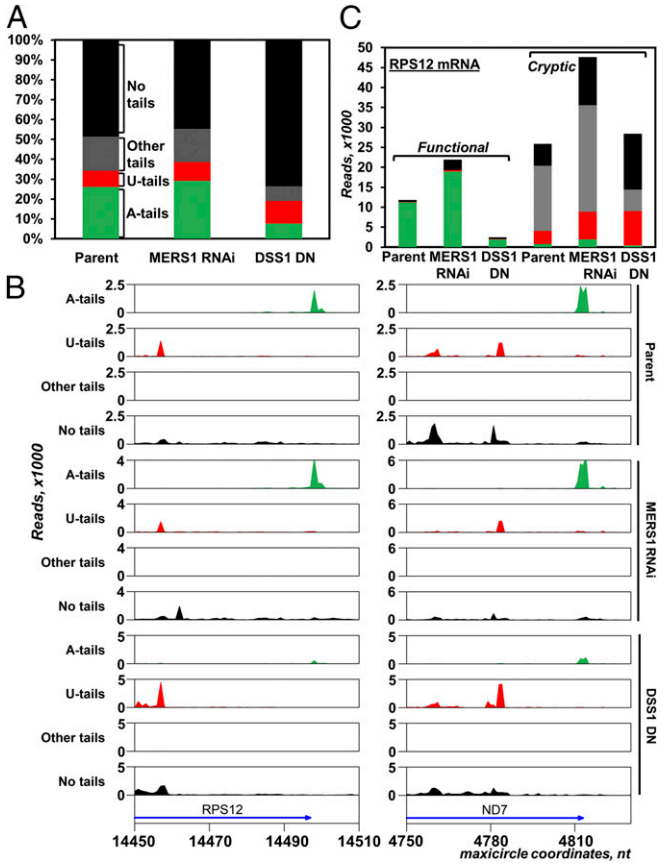

Fig. 6. mRNA 3′ adenylation is unaffected by MERS1 repression. (*A*) Relative global abundance of mRNA 3′ modifications. RNA linker ligation-based 3′ RACE was performed on parental, MERS1 RNAi, and DSS1 DN cells. The modifications were classified as A-tail (>90% As), U-tail (>90% Us), other (no nucleotide constitutes more than 90%), and unmodified. Read counts were normalized to a synthetic RNA spike. (*B*) Processing variants of individual transcripts clustered by tail type. For representative RPS12 and ND7 mRNAs, the last encoded nucleotide bearing the same tail was mapped to a respective gene (blue arrow). Read scale and maxicircle coordinates are indicated. (*C*) Tail composition of functional and truncated RPS12 mRNA 3′ ends. Color code is as in *A*.

Dataset S5). For all 20 tested canonical mRNAs and rRNAs, the closest antisense transcription start sites were detected within 0–19 nt (median 6 nt, each supported by at least 10 reads) of their mature 3′ ends (Dataset S5). Remarkably, antisense initiation signals were also observed near truncated mRNAs 3′ termini, which are often uridylated (−70 to −80 region) (Fig. 6*B* and ref. 16). To assess the size and heterogeneity of ncRNAs and the impact of MERS1 and DSS1 inhibition on antisense transcripts, we analyzed molecules complementary to pre-edited RPS12 (major strand) (33) and unedited MURF5 (encodes mitochondrial ribosomal protein uS3m on the minor strand) (29) pre-mRNAs by Northern blotting (Fig. 7*B*). The detected transcripts did not correspond to any annotated mRNA transcribed from the same strand and location and apparently lacked 3′ A-tails. Furthermore, in contrast to canonical mRNAs (Fig. 4), the ncRNAs were up-regulated in both MERS1 RNAi and DSS1 DN cells. While antisense accumulation is expected in the DSS1 DN background, a similar increase in MERS1 knockdown implicates the PPsome in destabilizing the nonadenylated antisense transcripts. In agreement with the 3′ RACE results, adenylation is apparently required for RNA stabilization by the PPsome.

To test whether antisense ncRNA can, in principle, impede highly processive DSS1 exonuclease activity, we reconstituted the mRNA 3′-processing reaction in vitro. Synthetic 5′-radiolabeled RNAs that resemble the 3′ regions of RPS12 and ND7 pre-mRNAs were hybridized with data-supported antisense RNA fragments and were incubated with affinity-purified active (WT) and inactive (DN) DSS1 3′–5′ exonuclease (Fig. 7 *C* and *D*, *Upper*). Both single-stranded fragments were processively degraded to 4- or 5-nt final degradation products with minor amounts of abortive products, which is consistent with RNase II-like DSS1 activity (13). Introducing partially dsRNA into the reaction induced strong and precise pausing 2–4 nt upstream of the antisense RNA 5′ end, but ∼30-nt shorter RNAs that resemble internal stops were also observed in vivo (Fig. 6*B*). To verify the formation of a duplex with a trimmed 3′ overhang, the reaction products were separated on native gel under conditions that retain all degradation products (Fig. 7 *C* and *D*, *Lower*). The DSS1 pausing before the duplex regions appears to be stochastic: The RNA hydrolysis-driven unwinding activity proceeds with some frequency into the double-stranded region or degrades the entire RNA to short oligonucleotides. The former pattern would be consistent with detection of truncated mRNA 3′ ends, while the latter explains the accumulation of mRNA precursors at significantly higher levels than mature mRNAs (14, 16). These in vitro experiments provide proof-of-principle support for the potential role of antisense transcription in the delineation of mature mRNA 3′ ends.

Discussion

The mitochondrion undergoes dramatic changes in function, size, and gene expression during the digenetic life cycle of *T. brucei*. The developmental variations in abundance, the 3′ modification state, and the extent of editing have been documented for most mitochondrial mRNAs (34), but few of these factors correlate with expected requirements for a specific protein at a particular life-cycle stage. Major advances in understanding mRNA editing, polyadenylation, and translation processes (31, 35) have left the decades-old notion of unregulated multicistronic transcription unperturbed. Likewise, the primary RNA cleavage by an endonuclease was assumed to produce monocistronic substrates for 3′ adenylation and editing. Although this scenario explains monophosphorylated 5′ and homogenous 3′ termini, the endonuclease identity and specificity determinants remained unsolved. The endonuclease model downplays transcriptional control of individual genes and presumes that precursor cleavage efficiency, mRNA adenylation, editing, and turnover ultimately dictate the steady-state levels of translation-competent mRNAs. By combining in vivo nucleic acid–protein cross-linking, genetic, proteomic, and in vitro reconstitution studies of mitochondrial RNA, polymerase, and mRNA 5′ and 3′ processing and editing complexes, we show that maxicircle genes are individually transcribed as 3′-extended precursors. We demonstrate that mRNA and rRNA 5′ termini are set by transcription initiation and are dephosphorylated by the PPsome. Biochemical and genetic data implicate MERS1 NUDIX hydrolase as the most likely PPsome subunit responsible for pyrophosphohydrolase activity. However, the autonomous MERS1 is catalytically inactive and requires an RNA-mediated association with the RESC to remove pyrophosphate in vitro. It seems likely that RESC recruitment serves as a two-pronged quality checkpoint to ensure that only target-bound MERS1 is catalytically active and to verify that RESC-bound pre-mRNA is properly adenylated and therefore is competent for internal editing. These conclusions are also supported by a stronger down-regulation of edited mRNAs than their pre-edited counterparts, such as *cyb* mRNA (Fig. 5*F*), or unedited transcripts. However, the specificity comes at a cost. The low efficiency of the MERS1-catalyzed reaction may be responsible for the rapid decay of mRNA precursors in contrast to structured rRNAs, which are less affected by MERS1 repression.

PPsome in vivo RNA-binding sites are predominantly located near the mRNA 5′ termini, and it seems probable that the MERS2 PPR subunit is responsible for RNA recognition and enabling MERS1 activity. Although maxicircles constitute only about 5% of kinetoplast DNA mass (36), their transcripts accounts for more than 65% of PPsome binding sites; only ∼1% belong to the highly diverse and abundant minicircle-encoded gRNAs, with the rest mapping to both genomes (Dataset S4). This correlation indicates

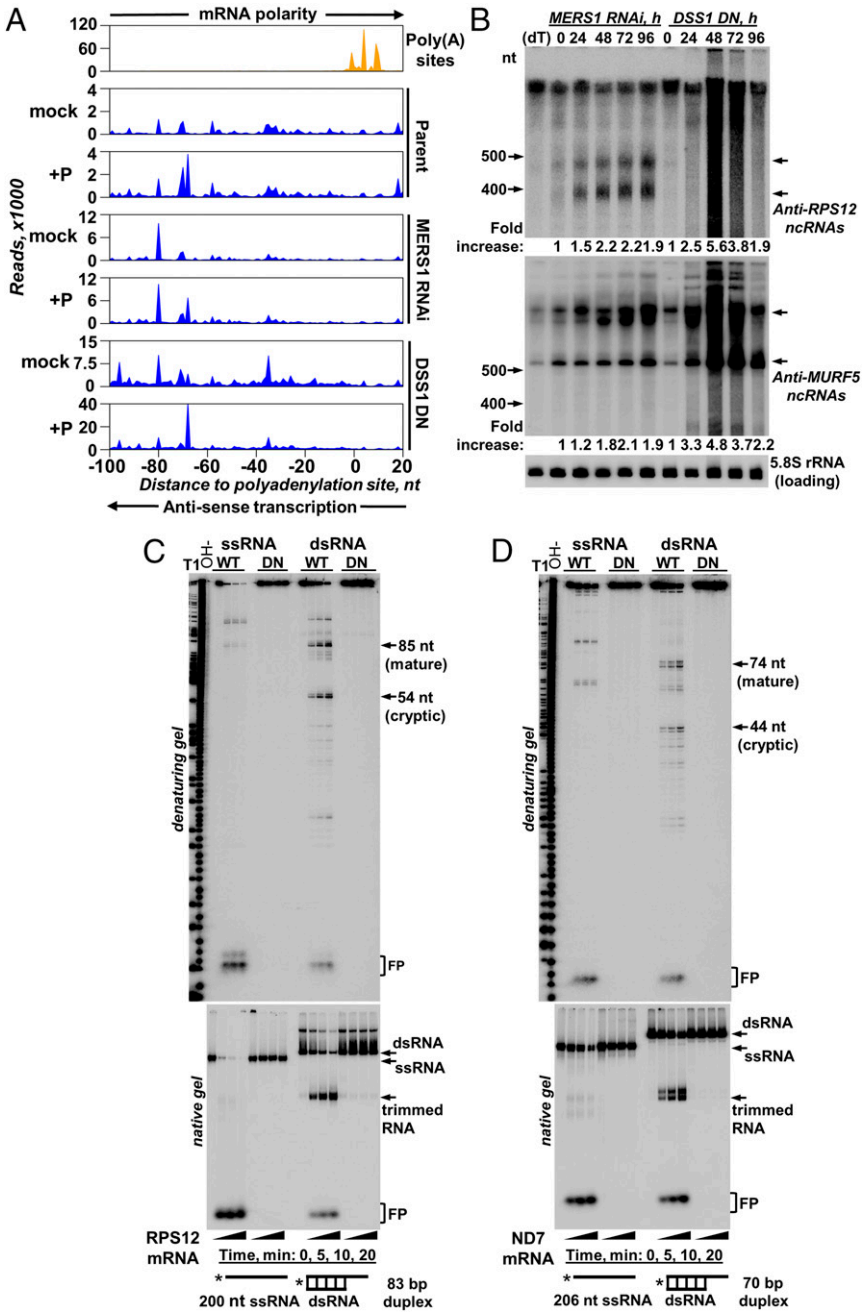

Fig. 7. Antisense transcription defines the mRNA 3′ end by blocking DSS1 exonuclease. (*A*) Mapping 5′ termini of antisense transcripts. A 5′ RACE was performed in the parental, MERS1 RNAi, and DSS1 DN cells. RNA was treated with 5′ polyphosphatase to capture mono- and triphosphorylated transcripts (+P) or was mock treated. Positions of canonical mRNA adenylation sites are shown in the top frame. The 5′ RACE reads for antisense RNAs were aligned to maxicircle sequences. Read counts located 100 nt downstream and upstream of the mapped polyadenylation site in each transcript were collected in 1-nt bins. The composite distribution of antisense RNA 5′ ends within annotated mRNA boundaries is shown by summation of coverage across all genes. The 3′ RACE-defined polyadenylation site is set as zero. (*B*) Detection of ncRNAs transcribed as antisense to RPS12 and MURF5 pre-mRNAs. Total RNA from MERS1 RNAi and DSS1 DN cells was analyzed by Northern blotting. Fold increase was calculated by the combining intensities of the indicated bands at each time point. (dT), RNA was treated with RNase H in the presence of oligo(dT) 20-mer to eliminate A-tails. Note unaltered migration patterns in the RNase H/oligo(dT) sample. (*C*) Antisense RNA-controlled 3′-end definition in vitro. Active (WT) and inactive (DN) DSS1 exonuclease variants were isolated from the mitochondrial fraction by TAP. Reactions with the 5′ radiolabeled single-stranded (ss) RPS12 mRNA fragment or preassembled partially dsRNAs were terminated by adding Proteinase K. Products were resolved on polyacrylamide denaturing (*Upper*) or native (*Lower*) gels. FP, final degradation products (4 or 5 nt). (*D*) The reactions shown in *C* performed with the ND7 mRNA fragment.

that gRNAs are not recognized by the PPsome and explains why these RNAs maintain transcription-incorporated 5′ triphosphate. Conversely, PPsome-bound primary 5′ ends of maxicircle transcripts are converted to the monophosphate form. The essentiality of pyrophosphate hydrolysis for mRNA maintenance underscores the fundamentally different mechanisms that stabilize maxicircle-encoded mRNAs and minicircle-encoded gRNAs. The mature 3′-uridylated gRNAs are directly bound to the GRBC (14, 17), a discrete module within the larger RESC (Fig. 3 and refs. 18 and 37). Initially defined as the RNA-binding component of the RNA-editing

holoenzyme, the RESC also interacts with KPAC. Our study demonstrates a critical role of the 5′ PPsome in protecting mRNA against degradation by DSS1 exonuclease, which is responsible for both 3′ processing and the decay of all mitochondrial RNA species (13, 16). The RESC-mediated contacts between the PPsome and KPAC strongly suggest that proximity of monophosphorylated 5′ ends and adenylated 3′ ends may be an essential mRNA-stabilization element. Given the gene-specific transcription initiation, the RNAs spanning gene boundaries (12, 38) apparently represent 3′ heterogeneous precursors that intrude into downstream coding sequences (16). Therefore, the 3′-end processing pathway should include a mechanism by which the highly processive 3′–5′ precursor degradation is blocked at a specific point before mRNA adenylation or rRNA uridylation. To that end, we have identified ubiquitous antisense transcripts that initiate near the functional mRNA 3′ end and recapitulated a plausible pausing mechanism for 3′–5′ degradation in vitro. In this stochastic event, the 5′ end of the antisense ncRNA dictates the position of the mRNA's 3′ end and generates a substrate for the KPAC. In contrast to mRNAs, the antisense noncoding transcripts are up-regulated in MERS1 knockdown. It seems plausible that the PPsome surveils the steady-state levels of antisense transcripts, but the mechanism remains to be established.

In organisms with few mitochondrial promoters and predominantly polycistronic transcription (yeast, mammals), transcriptional control seems to be of limited importance (1). Along with plastid-like glycosomal enzymes (39) and multiple PPR proteins (40), mitochondrial transcription driven by multiple promoters joins the repertoire of plant-like traits and indicates that trypanosomes may have possessed plastids and photosynthesis at some point in their evolution. It is now conceivable that transcription, in addition to internal editing and 3′ adenylation (14, 16, 25), plays a significant role in developmental regulation of mitochondrial gene expression. In summary, we have demonstrated that mitochondrial pre-mRNAs and rRNAs are transcribed individually and have revealed the mechanisms by which 5′ and 3′ termini are produced and mature mRNAs are stabilized.

Methods

T. brucei subsp. *brucei* strain Lister 427 29-13 (TetR T7RNAP) is a procyclic form cell line that expresses T7 RNA polymerase (T7RNAP) and tetracycline repressor (TetR). Strain Lister 427 29-13 (TetR T7RNAP) was derived by sequential transfections of the procyclic Lister 427 strain (NR-42010; BEI Resources) (41). This cell line was maintained in SDM-79 medium (Life Technologies, custom order part no. ME090164 P1) supplemented with neomycin, hygromycin, and 10% FBS at 27 °C. A detailed description of methods employed in this study is provided in *SI Appendix*.

ACKNOWLEDGMENTS. We thank members of the I.A. laboratory for valuable discussions, Ken Stuart for providing pSM06 and pSM07 plasmids, and Laurie Read for the RGG2 antibody. This work was supported by NIH Grants R01 AI113157 (to I.A.), R01 GM074830 and R01 GM106003 (to L.H.), and R01 AI091914 and R01 AI101057 (to R.A.).

1. Lipinski KA, Kaniak-Golik A, Golik P (2010) Maintenance and expression of the S. cerevisiae mitochondrial genome–From genetics to evolution and systems biology. *Biochim Biophys Acta* 1797:1086–1098.
2. Bestwick ML, Shadel GS (2013) Accessorizing the human mitochondrial transcription machinery. *Trends Biochem Sci* 38:283–291.
3. Binder S, Stoll K, Stoll B (2016) Maturation of 5′ ends of plant mitochondrial RNAs. *Physiol Plant* 157:280–288.
4. Ojala D, Montoya J, Attardi G (1981) tRNA punctuation model of RNA processing in human mitochondria. *Nature* 290:470–474.
5. Pearce SF, et al. (2017) Regulation of mammalian mitochondrial gene expression: Recent advances. *Trends Biochem Sci* 42:625–639.
6. Aphasizhev R, Aphasizheva I (2011) Uridine insertion/deletion editing in trypanosomes: A playground for RNA-guided information transfer. *Wiley Interdiscip Rev RNA* 2:669–685.
7. Blum B, Bakalara N, Simpson L (1990) A model for RNA editing in kinetoplastid mitochondria: "Guide" RNA molecules transcribed from maxicircle DNA provide the edited information. *Cell* 60:189–198.
8. Michelotti EF, Harris ME, Adler B, Torri AF, Hajduk SL (1992) *Trypanosoma brucei* mitochondrial ribosomal RNA synthesis, processing and developmentally regulated expression. *Mol Biochem Parasitol* 54:31–41.
9. Grams J, et al. (2002) A trypanosome mitochondrial RNA polymerase is required for transcription and replication. *J Biol Chem* 277:16952–16959.
10. Simpson AM, Suyama Y, Dewes H, Campbell DA, Simpson L (1989) Kinetoplastid mitochondria contain functional tRNAs which are encoded in nuclear DNA and also contain small minicircle and maxicircle transcripts of unknown function. *Nucleic Acids Res* 17:5427–5445.
11. Koslowsky DJ, Yahampath G (1997) Mitochondrial mRNA 3′ cleavage/polyadenylation and RNA editing in *Trypanosoma brucei* are independent events. *Mol Biochem Parasitol* 90:81–94.
12. Read LK, Myler PJ, Stuart K (1992) Extensive editing of both processed and preprocessed maxicircle CR6 transcripts in Trypanosoma brucei. *J Biol Chem* 267:1123–1128.
13. Suematsu T, et al. (2016) Antisense transcripts delimit exonucleolytic activity of the mitochondrial 3′ processome to generate guide RNAs. *Mol Cell* 61:364–378.
14. Aphasizheva I, Aphasizhev R (2010) RET1-catalyzed uridylylation shapes the mitochondrial transcriptome in *Trypanosoma brucei*. *Mol Cell Biol* 30:1555–1567.
15. Mattiacio JL, Read LK (2008) Roles for TbDSS-1 in RNA surveillance and decay of maturation by-products from the 12S rRNA locus. *Nucleic Acids Res* 36:319–329.
16. Zhang L, et al. (2017) PPR polyadenylation factor defines mitochondrial mRNA identity and stability in trypanosomes. *EMBO J* 36:2435–2454.
17. Weng J, et al. (2008) Guide RNA-binding complex from mitochondria of trypanosomatids. *Mol Cell* 32:198–209.
18. Aphasizheva I, et al. (2014) RNA binding and core complexes constitute the U-insertion/deletion editosome. *Mol Cell Biol* 34:4329–4342.
19. Simpson AM, Neckelmann N, de la Cruz VF, Muhich ML, Simpson L (1985) Mapping and 5′ end determination of kinetoplast maxicircle gene transcripts from Leishmania tarentolae. *Nucleic Acids Res* 13:5977–5993.
20. Ignatochkina AV, Takagi Y, Liu Y, Nagata K, Ho CK (2015) The messenger RNA decapping and recapping pathway in Trypanosoma. *Proc Natl Acad Sci USA* 112:6967–6972.
21. Aphasizhev R, Aphasizheva I, Nelson RE, Simpson L (2003) A 100-kD complex of two RNA-binding proteins from mitochondria of Leishmania tarentolae catalyzes RNA annealing and interacts with several RNA editing components. *RNA* 9:62–76.
22. Neilson KA, Keighley T, Pascovici D, Cooke B, Haynes PA (2013) Label-free quantitative shotgun proteomics using normalized spectral abundance factors. *Methods Mol Biol* 1002:205–222.
23. Roux KJ, Kim DI, Raida M, Burke B (2012) A promiscuous biotin ligase fusion protein identifies proximal and interacting proteins in mammalian cells. *J Cell Biol* 196:801–810.
24. Bhat GJ, Souza AE, Feagin JE, Stuart K (1992) Transcript-specific developmental regulation of polyadenylation in *Trypanosoma brucei* mitochondria. *Mol Biochem Parasitol* 52:231–240.
25. Etheridge RD, Aphasizheva I, Gershon PD, Aphasizhev R (2008) 3′ adenylation determines mRNA abundance and monitors completion of RNA editing in T. brucei mitochondria. *EMBO J* 27:1596–1608.
26. Aphasizheva I, Maslov D, Wang X, Huang L, Aphasizhev R (2011) Pentatricopeptide repeat proteins stimulate mRNA adenylation/uridylation to activate mitochondrial translation in trypanosomes. *Mol Cell* 42:106–117.
27. Kao CY, Read LK (2005) Opposing effects of polyadenylation on the stability of edited and unedited mitochondrial RNAs in Trypanosoma brucei. *Mol Cell Biol* 25:1634–1644.
28. Aphasizheva I, Maslov DA, Aphasizhev R (2013) Kinetoplast DNA-encoded ribosomal protein S12: A possible functional link between mitochondrial RNA editing and translation in *Trypanosoma brucei*. *RNA Biol* 10:1679–1688.
29. Ramrath DJF, et al. (September 13, 2018) Evolutionary shift toward protein-based architecture in trypanosomal mitochondrial ribosomes. *Science*, 10.1126/science.aau7735.
30. McLennan AG (2006) The Nudix hydrolase superfamily. *Cell Mol Life Sci* 63:123–143.
31. Read LK, Lukeš J, Hashimi H (2016) Trypanosome RNA editing: The complexity of getting U in and taking U out. *Wiley Interdiscip Rev RNA* 7:33–51.
32. Maslov DA, Simpson L (1992) The polarity of editing within a multiple gRNA-mediated domain is due to formation of anchors for upstream gRNAs by downstream editing. *Cell* 70:459–467.
33. Maslov DA, et al. (1992) An intergenic G-rich region in *Leishmania tarentolae* kinetoplast maxicircle DNA is a pan-edited cryptogene encoding ribosomal protein S12. *Mol Cell Biol* 12:56–67.
34. Kirby LE, Sun Y, Judah D, Nowak S, Koslowsky D (2016) Analysis of the Trypanosoma brucei EATRO 164 bloodstream guide RNA transcriptome. *PLoS Negl Trop Dis* 10:e0004793.
35. Aphasizheva I, Aphasizhev R (2015) U-insertion/deletion mRNA-editing holoenzyme: Definition in sight. *Trends Parasitol* 32:144–156.
36. Muhich ML, Simpson L, Simpson AM (1983) Comparison of maxicircle DNAs of Leishmania tarentolae and Trypanosoma brucei. *Proc Natl Acad Sci USA* 80:4060–4064.
37. Ammerman ML, et al. (2012) Architecture of the trypanosome RNA editing accessory complex, MRB1. *Nucleic Acids Res* 40:5637–5650.
38. Feagin JE, Jasmer DP, Stuart K (1985) Apocytochrome b and other mitochondrial DNA sequences are differentially expressed during the life cycle of Trypanosoma brucei. *Nucleic Acids Res* 13:4577–4596.
39. Hannaert V, et al. (2003) Plant-like traits associated with metabolism of Trypanosoma parasites. *Proc Natl Acad Sci USA* 100:1067–1071.
40. Aphasizhev R, Aphasizheva I (2013) Emerging roles of PPR proteins in trypanosomes: Switches, blocks, and triggers. *RNA Biol* 10:1495–1500.
41. Wirtz E, Leal S, Ochatt C, Cross GA (1999) A tightly regulated inducible expression system for conditional gene knock-outs and dominant-negative genetics in Trypanosoma brucei. *Mol Biochem Parasitol* 99:89–101.